Review

International Journal of Modern Physics B
Vol. 27, No. 19 (2013) 1330013 (28 pages)

DOI: 10.1142/S0217979213300132

World Scientific
www.worldscientific.com

INDUCED MAGNETISM AT OXIDE INTERFACES

JACOBO SANTAMARIA*, JAVIER GARCIA-BARRIOCANAL,
ZOUHAIR SEFRIOUI and CARLOS LEON

GFMC, Departamento Fisica Aplicada III, Universidad Complutense Madrid
28040 Madrid, Spain
**jacsan@fis.ucm.es*

Received 13 June 2013
Accepted 14 June 2013
Published 3 July 2013

Interfaces between correlated oxides are attracting great interest. Electron correlations give rise to novel forms of couplings between electronic ground states at both sides of the interface. The bonding discontinuity at the interface between magnetic and nonmagnetic oxides is at the origin of a form of low dimensional magnetism in the otherwise nonmagnetic material. Its origin is the splitting of its bands due to the hybridization with the exchange split bands of the magnetic material. This induced magnetism could find interesting functionalities in devices with operation controlled by the interface such as tunnel or field effect devices of interest in spintronics.

Keywords: Oxide interfaces; magnetism; superconductivity.

PACS numbers: 73.20.-r, 75.70.Ch, 74.78.Fk

1. Introduction

Complex transition metal oxides are a wide family of materials which contain elements with incomplete d shells, what gives rise to different forms of magnetic interactions. Almost every electronic or lattice groundstate of solid matter can be found including superconductivity, ferromagnetism, antiferromagnetism, ferroelectricity, multiferroicity etc.[1,2] Distinct members of this class of materials are high T_c superconductors and colossal magnetoresistance manganites which have gathered one of the strongest research efforts in the history of science in terms of number and impact of research articles and number of researchers involved. Many complex oxides share a common perovskite structure where the basic building block is the oxygen octahedron surrounding the transition metal ion. The strong crystal (electric) field generated by the oxygen ions act on the otherwise 5 fold degenerate d levels of the transition metal ion splitting them in e_g and t_{2g} levels which are double and triple degenerate respectively. d orbitals are directional and their overlap mediated by the oxygen p orbitals is weak what yields the narrow d bands with large

effective masses. Electrons have thus low mobilities and strongly feel the lattice giving rise to the strong electron lattice coupling (Jahn–Teller) which may further split the degeneracy of crystal field levels. But more importantly, narrow and directional bands poorly screen the electrostatic repulsion between electrons. The unscreened Coulomb interaction gives rise to strong correlations in the electron system.[2] As a result, the electronic properties cannot be described within conventional one electron band pictures. In a system with one electron per site, expected to be a metal in the one electron band theory of solids, the electrostatic repulsion opens a gap at the Fermi energy. This is the so called Mott gap. Strong electron correlations underlie the strong entanglement between the various interactions in these materials with a multiplicity of competing phases with similar characteristic energies. This is probably at the origin of the rich phase diagrams and of the inhomogeneous ground states displayed by many transition metal oxides.[3] Most likely this competition between interactions also underlies the complex (often giant) collective responses exhibited by these materials upon small perturbations whose understanding and prediction remains a major challenge of condensed matter physics for the years to come.[4]

In recent years there has been a lot of activity directed to the growth of heterostructures combining complex transition metal oxides. The strongly correlated nature of the conduction electrons underlying the interplay between the various degrees of freedom is at the origin of the rich variety of new effects and phenomena found at oxide interfaces. The fabrication technique of these oxide heterostructures has reached a level of control comparable to the semiconductor technology and interfaces can be grown with atomic precision allowing the lattices with dissimilar materials to match with a high degree of crystalline perfection. Much in the same way than in the history of semiconductor devices, where interesting effects and phenomena and even novel states of matter have been found at their rather inert interfaces, oxide interfaces constitute an appealing playground for the exploration of exciting new physics.[5,6] The broken symmetry at the interface between dissimilar correlated oxides underlies the nucleation of emergent electronic phases with unexpected properties far from those of the constituent oxides. Charge density n, repulsion energy U, and band width W, the important parameters critically controlling the properties of correlated oxides are known to vary at interfaces providing interesting avenues to tailor their electronic structure. On the one hand, charge density is known to leak across interfaces as the result from differences between electrochemical potentials, varying smoothly across the interface over the Thomas Fermi screening length. Repulsive interaction U is also known to depend critically on the ionic environment and band width W is controlled by bond reconstruction (length and angle) at the interface. Since many of these oxides are doped insulators in the vicinity of a metal to insulator transition, the charge density profile at the interface has a critical influence in nucleating novel phases at (the most stable) individual values in a process called electronic reconstruction.[7] Furthermore, since not only n but also U and W change at the interface lattice discontinuity, novel phases

nucleate at individual values of n, U and W with unexpected spin and conducting properties in a more general scenario named electronic metamorphosis.[5]

A paradigmatic example of unexpected electronic states appearing at oxide interfaces is the metallic low dimensional electronic state at the LAO/STO interface between two band insulators.[8,9] It has been proposed that electrons are transferred to the interface as the result of the polarity mismatch between the (100) planes of the LAO (polar) and the STO (nonpolar). Within this scenario, charge is transferred from the surface of the LAO to the interface to avoid divergence of the electrostatic energy stored in the LAO when its thickness is increased.[10,11] Alternative scenarios have been proposed related to the presence of oxygen vacancies[12–15] or to intermixing processes[16–18] which dope the interface layer with electrons. The carrier density of the 2D electron gas is electrically tuneable[19,20] and its ground state can be controlled to change from superconducting[21] to (ferro) magnetic[22] just by changing the carrier density. This finding has triggered the launch of a truly new research field aimed at designing and controlling the electronic structure at the interfaces. The wide variety of possibilities offered by oxide interfaces to stabilize new electronic ground states holds an appealing technological promise of new device concepts, which relies on being able to manipulate and control them with external stimuli.

At interfaces the discontinuity in the bonding structure may result in interesting forms of interfacially induced magnetism. The rationale is as follows. At interfaces between magnetic and nonmagnetic species, induced moments due to hybridization become important in the ultrathin limit when layer thickness is comparable to lattice spacing. The antecedents to these magnetically induced moments are found in the field of metallic superlattices. At the interface between transition metals the electron gas of the nonmagnetic element is spin polarized via an indirect exchange interaction, which has an oscillatory character. This is the interaction responsible for the oscillatory coupling of metallic superlattices exhibiting giant magnetoresistance.[23] There are three important length scales involved. When the thickness of the nonmagnetic spacer is of the order of or smaller than its electron mean free path, spin dependent scattering originates the giant magnetoresistance. Its magnitude is influenced by interface roughness due to spin dependent scattering at the interface.[24–29] Oscillatory coupling itself evolves with the inverse of the Fermi wave vector. On the other hand, when the thickness on the spacer metal becomes comparable to lattice spacing a different mechanism comes into play related to the hybridization between the bands of both species. XMCD experiments have supplied evidence for this form of induced magnetism at interfaces between 3*d* ferromagnets (Fe, Co, Ni) and 3*d* (Pt, Cu, V, Ti)[30] and 5*d* (W, Ir)[31,32] elements. The explanation put forward[33] relies on the strong hybridization between the minority band of the ferromagnet and the spin down band of the nonmagnetic element. As a result the hybridized bands are shifted down in energy (as compared to the nonhybridized bands which are further apart in energy) and become more filled, which results in a net spin moment that is aligned antiparallel to the ferromagnetic moment. The induced moments significantly determine various magnetic properties like the

magnetotransport properties,[34] the magneto-optic response,[35] and the magnetic anisotropy.[36,37]

The reconstructed bond at oxide interfaces constitutes a new superexchange path between different elements. The different orbital structure and filling, which may be influenced by charge transfer or strain, may cause profound changes of the spin–spin interaction at the interface determining its sign (ferromagnetic versus antiferromagnetic respect to the inductor magnetic moment). It is known that in these oxides in which the orbital degree of freedom is quenched the spin–spin interaction is determined by the orbital structure and filling.[1,2] In transition metal oxides, crystal field interaction mixes wave functions in such a way that the z component of the orbital angular momentum is zero. Thus, magnetic structure is largely governed by spins and their interactions, although in some cases the small spin orbit interaction of transition metal ions can partially restore the orbital component. Spin interaction is controlled by real and/or virtual charge transfer processes. For orthogonal nonoverlapping orbitals charge transfer is not allowed and the interaction is by direct potential exchange which is ferromagnetic as in the intra-atomic Hund coupling. On the other hand, for overlapping orbitals (through the p states of an intermediate oxygen anion) the charge transfer process may be real as in double exchange or virtual as in superexchange. Orbital geometry and filling determines the spin–spin structure according to the Goodenough–Kanamori rule,[38,39] a hierarchy which determines the sign of the interaction as a function of filling and overlap according to the Pauli Exclusion Principle. If a superexchange process connects two partially filled orbitals Pauli Exclusion Principle requires that the superexchange process is AF. If on the other hand, one of the levels is partially filled and the other is empty the superexchange interaction is ferromagnetic as in double exchange.

Epitaxial strain is a main player in this game in determining the orbital occupancy at the interface. It has been known already for many years that epitaxial strain can modify the occupation of the orbitals at the interface.[40] The orbital lobes tend to accommodate along the elongated dimension, such that in plane tensile strain promotes $e_g x^2 - y^2$ or $t_{2g} xy$ in plane occupation while compressive strain promotes e_g $3z^2 - r^2$ or t_{2g} xz or yz out of plane orbital occupation. Changes in orbital occupancy determine spin–spin interaction and supply a path to modify interfacial magnetism. It turns out that oxide heterostructures are able to accommodate large amount of strain as compared to their semiconductor counterparts without breaking into islands. For example, the epitaxially coherent growth of a few unit cells of fluorite yttria stabilized zirconia on perovskite $SrTiO_3$ despite a 7% lattice mismatch.[41] Such a high level of strain keeping epitaxy has to our knowledge never been achieved in semiconductors, and is probably connected with the ability of the oxygen sublattice to distort, rotate or tilt. This amplifies the opportunity of using strain to modify the magnetic structure of interfaces through its effect on orbital structure.[42]

Probing interface magnetism is a difficult matter for a variety of reasons. Interfaces usually are a small mass fraction of the sample what makes SQUID or VSM magnetometry not suited for its detection. Interfaces are buried and usually shape anisotropy sets in plane magnetization directions which rules out using contact probes like magnetic force microscopy. Moreover, interfacial magnetism is a ground state induced in a nonmagnetic oxide as a result of an interfacial bond with a magnetic oxide. This also rules out polarized neutron reflectometry which will be dominated by the most abundant magnetic species. We thus need a technique capable of probing the magnetic state with element sensitivity, such as X-ray absorption with polarization analysis (XMCD). The use of circularly polarized photons provides access to the magnetic structure of the valence band. We offer here a survey of the very basic ideas and refer the reader to a more specialized text for an in depth review.[43,44] Absorption of circularly polarized photons transfers their angular momentum to the photoelectrons, which will be spin polarized in a way determined by the spin orbit coupling of the core level. In particular, transitions between the $2p$ and $3d$ levels give rise to resonant X-ray scattering what increases the absorption (cross section) intensity by more than a factor of 20 as compared to the absorption between p and s levels. Comparing the absorption of circularly polarized photons with opposite helicities provides direct access to the magnetic state of the d shell allowing direct determination of the spin and orbital moment in a way which is element specific. The $2p$ level is spin orbit split in $2p_{3/2}$ (L3) and $2p_{1/2}$ levels (L2). In a first step one can think that the circularly polarized photons transfer its angular momentum ($\pm\hbar$) to the excited photoelectrons. Now since L3 and L2 levels have opposite spin orbit coupling, for a given helicity (say minus, for which photons are left polarized) photoelectrons will have an angular momentum increased by $\hbar$. Depending on whether they are coming from the L3 or the L2 level, for which spin orbit coupling is $l+s$ or $l-s$ respectively, they will be mostly spin up or spin down respectively. In other words, for left polarized photons L3 absorption probes the spin up band and L2 absorption probes the spin down band (with different transition rates). Conversely, given a core level absorption say L3, left and right polarized photons probe spin up and spin down bands respectively. The spin split density of states of a magnetic d band will act as a detector of the spin polarization of the excited photoelectrons. Moreover, if the d band has an angular momentum, it will also "analyze" the angular momentum of the excited photoelectrons. The difference in absorption between both helicities thus provides a measure of the orbital and spin polarization of the band in a way determined by the selection rules, which determine spin and orbital moment as a function of the integrated intensities under the dichroic signal at the two absorption edges. The alignment of the orbital moment respect to the spin moment is determined mostly by the filling of the $3d$ band according to the third Hund's rule, although breakdown of the rule is found near to half filling.

In this paper we review recent progress on magnetic ground states induced by the superexchange interaction at interfaces between magnetic and nonmagnetic oxides.

We will explicitly distinguish two related scenarios. In one case we will consider magnetism induced in a layer with some form of pre-existing magnetic order. This is the case of the cuprate/manganite or the ferrite/manganite interfaces. Parent compounds of cuprates are known to be antiferromagnets and strong antiferromagnetic correlations persist in the lightly doped compounds. At cuprate manganite interfaces charge transfer effects reduce the hole doping and increase the strength of the antiferromagnetic correlations. $LaFeO_3$, on the other side is an antiferromagnetic Mott insulator. In both cases, induced magnetism consists essentially in a canting of a previously existing antiferromagnetic Cu or Fe lattice. On the other hand, we will also consider the case of induced magnetism at titanate/manganite interfaces. $SrTiO_3$ is a band insulator with a diamagnetic ground state due to the Ti^{4+} ions. Although magnetic moments can be induced by electron doping of the titanates, none of the doped titanates formed at our interfaces are to our knowledge magnetic in their bulk form. Thus, induced magnetism in these titanates is an even more striking and exotic phenomenon.

2. Magnetism at Cuprate Manganite Interfaces

The interfaces between ferromagnetic (half metallic) manganites and high T_c superconductors have focused a lot of interest in recent years. The good lattice matching and chemical compatibility between both materials have allowed the growth of atomically sharp interfaces, at which interesting effects result from the interplay between the two antagonistic ground states. In the following we describe this interplay with special focus on the induced magnetism.

The bonding reconstruction at the interface supplies an interesting additional strategy to tailor interfacial magnetism at the boundary between manganite and cuprate oxides. The new bond perpendicular to the interface constitutes a new 180 degrees superexchange path which transmits a magnetic interaction into the cuprate. The sign of the coupling is determined by orbital symmetry and filling. This effect was discovered at cuprate manganite interface by B. Keimer's group at the Max Planck Institute.[45,46] The dichroic signal of Cu atoms at the interface evidences an induced magnetic moment antialigned to the neighboring Mn moments. The magnetic signal of the Cu dies with the Mn moment when temperature is increased evidencing that Cu moment is in fact induced by the magnetism of the manganite.

The antiferromagnetic superexchange interaction through the interface competes with the antiferromagnetic superexchange between neighboring Cu atoms which results from the depletion of holes at the interface due to the missing CuO chains. The former causes a canting of the antiferromagnetic Cu lattice to attain the measured 0.2 μ_{Bohr}/Cu atom measured by the dichroism experiment. The antiferromagnetic coupling seems at first sight inconsistent with Goodenough–Kanamori rule. The conduction electrons of the cuprate reside in the x^2–y^2 orbital, but the active orbital at the interface is the $3z^2$–r^2 orbital which is completely filled in the

bulk. The Cu–O–Mn superexchange interaction would be thus mediated by virtual charge transfer from the Cu $3z^2$–r^2 orbital into the half-filled $3z^2$–r^2 orbital in the manganite, which should be ferromagnetic due to the Cu intra-atomic Hund rule interaction. The antiferromagnetic coupling observed experimentally constitutes a direct indication that the electronic reconstruction at the interface encompasses also an orbital reconstruction where orbital occupancy changes respect to bulk values. Linear dichroism experiments comparing fluorescence signal (more sensitive to the bulk) and total electron yield (more sensitive to the interface) has shown significant polarization of the $3z^2$–r^2 orbitals of the cuprates indicating that some hole population, contrary to the bulk where holes reside in the x^2–y^2 orbitals. It has been proposed that orbital reconstruction results from covalent bonding in the direction perpendicular to the interface. Spin up $3z^2$-r^2 molecular hybrids with a strong Hund coupling to t_{2g} Mn electrons, have their energy reduced due to hybridization. As a result of the difference in electrochemical potential the spin up antibonding orbital is higher in energy than the Cu x^2–y^2 hybrids where the holes reside. This causes transfer of holes from the x^2–y^2 orbitals to the $3z^2$–r^2 orbitals, what accounts for the orbital reconstruction.

Recent studies on $La_{0.7}Ca_{0.3}MnO_3$ (LCMO)/$YBa_2Cu_3O_7$ (YBCO) epitaxial heterostructures have evidenced suppression of the superconducting critical temperature over length scales much larger (1–2 orders of magnitude) than the coherence length of the cuprate.[47–49] Figure 1(a) shows the resistance curves of a series of LCMO/YBCO superlattices with fixed thickness of the manganite and changing the thickness of the cuprate in unit cell steps. F/S/F trilayers and heterostructures were grown by sputter deposition in pure oxygen pressure[47–49] on (100) $SrTiO_3$ substrates. A strong suppression of the critical temperature can be seen when the thickness of the YBCO is reduced. Figure 1(b) shows the evolution of the critical temperature of trilayers with magnetic (LCMO) and $PrBa_2Cu_3O_7$ (PBCO) bottom and top layers sandwiching the superconducting layers. Notice that superconductivity is further suppressed in heterostructures involving a magnetic material suggesting a proximity effect which occurs over a very long length scale (10 nm), orders of magnitude larger than the superconducting coherence length (0.1–0.3 nm in the c direction). This can be hardly explained in terms of a (singlet) proximity effect given the high spin polarization of the manganite and the sub-nanometer coherence length of the cuprate. In the ferromagnet (F)/superconductor (S) proximity effect[50,51] the superconducting condensate leaks into the ferromagnet, so that Cooper pairs directly experience the exchange interaction.[52–60] The effect is short range, and its length-scale shortens when the spin polarization of the ferromagnet increases, vanishing in the limit of full spin polarization of a half metal. Superconductivity is also suppressed in the superconducting layer over the superconducting coherence length. Other explanations in terms of (self) diffusion of spin polarized quasiparticles[61] or induction of a triplet superconductivity component[62,63] also do not account for the long length scale of the superconductivity suppression in the cuprate. The effect of the induced magnetism at the interface is to create a spin

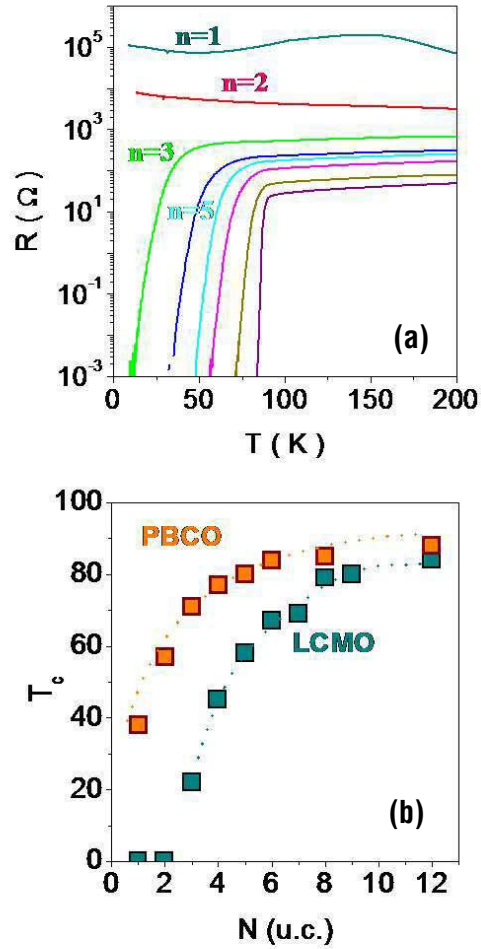

Fig. 1. (Color online) (a) Resistance curves of LCMO/YBCO superlattices with fixed thickness of the manganite of 15 unit cells and changing the thickness of the cuprate in unit cell steps. (b) Critical temperature obtained from the zero resistance value (in a linear scale) of LCMO/YBCO/LCMO trilayers with magnetic (LCMO) and nonmagnetic $PrBa_2Cu_3O_7$ (PBCO) top and bottom layers. Figures adapted from Refs. 47 and 48.

polarization in the electron gas of the cuprate over a short distance from the interface, which, as it has been theoretically shown recently, may have a drastic effect in suppressing superconductivity in ultrathin layers. In fact, as we discuss later, this induced spin polarization is responsible from an anomalous proximity effect reported previously in manganite cuprate heterostructures.

In the following we will argue that, in fact, the low dimensional Cu magnetism induced at both interfaces resulting from the atomic reconstruction imposed by the epitaxial growth process is at the origin of the superconductivity suppression. To describe the interface structure we will focus on a series of F/S/F trilayers with

fixed 15 nm thick top and bottom LCMO layers while the YBCO thickness ranges between 7 and 47 nm. Samples were grown by high pressure pure oxygen sputtering, a technique which has proven the growth of oxides layers with good epitaxial properties.[64–66] Samples with YBCO thicker showed weaker superconductivity sup-

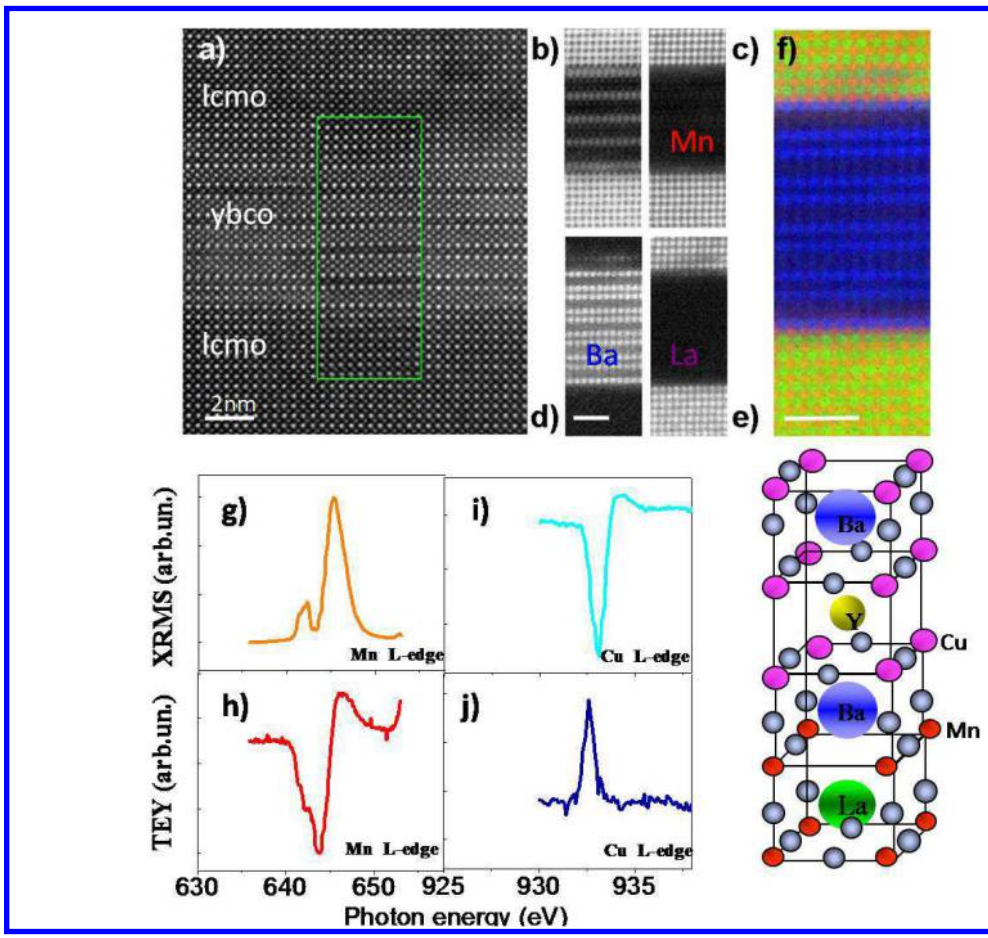

Fig. 2. (Color online) (a) High resolution image of a LCMO/YBCO/LCMO trilayer. Z-contrast images were obtained at Oak Ridge National Laboratory in a Nion UltraSTEM operated at 100 kV and equipped with a 5th order corrector and a Gatan Enfina spectrometer to allow simultaneous imaging and electron energy loss spectroscopy (EELS). EELS elemental maps using normalized integrated intensities for the O K (b), Mn $L_{2,3}$ (c), Ba $M_{4,5}$ (d) and La $M_{4,5}$ (e). The color map of panel (f) has been produced by overlaying the Ba image (blue) and the Mn image (red), and the La image (green). The scale bar in all cases represents 2 nm. The sketch represents the growth mode with missing CuO chains at the interface. X-ray resonant magnetic scattering (XRMS) and total electron yield (TEY) XMCD spectra at the Mn absorption edge [(g) and (h)] and at the Cu absorption edge [(i) and (j)] at 30 K. XRMS (g) and TEY (h) at 645.5 eV for the Mn L-edge and at 932.5 eV for the Cu L-edge (i) XRMS and j) TEY) with the beam oriented parallel to the external field and making an angle of 10 degrees with the sample surface. Figures adapted from Ref. 74.

pression until for samples thicker than 15 nm bulk T_c is recovered, ruling out oxygen deficiency as the origin of T_c reduction.[67–70] X-ray and neutron nuclear depth profiles (not shown) indicate that the roughness of the top LCMO layer is larger than those of the bottom LCMO layer and that the average magnetization is reduced. An additional suppression of the top LCMO layer magnetization is observed at the interface with YBCO, which has previously been interpreted to result from electron transfer from the manganite into the cuprate.[71,72] Interface structure and composition examined by aberration corrected STEM show good epitaxial properties and coherent growth. EELS spectrum images were acquired to investigate the interface structure. Figure 2(a) displays a high magnification Z contrast STEM image of a LCMO (top)/YBCO (middle)/LCMO (bottom) trilayer. The darker planes corresponding to CuO chains of YBCO are missing at both interfaces. Elemental maps corresponding to the O K, Mn $L_{2,3}$, Ba $M_{4,5}$, and La $M_{4,5}$ edges are shown in Figs. 2(b)–2(e), respectively. The atomic lattices of all these elements are clearly resolved. Interestingly, the LCMO layer looks chemically wider on the Mn image than on the La map. These maps indicate a (BaO) atomic plane termination for both the top and bottom interfaces of the cuprate and MnO_2 of the manganite at both interfaces. These results are consistent with *both* interfaces displaying the same termination with a plane sequence YBCO–BaO–CuO_2–Y–CuO_2–BaO–MnO_2–(La, Ca O)–LCMO as reported previously by some of us in similar samples.[71] This observation is more evident when the compositional maps are coloured and overlay as done in Fig. 2(f): a blue BaO plane faces a red MnO_2 plane for both the top and bottom interfaces.

Soft X-rays in the energy range of Mn and Cu L-absorption edges were used to obtain element specific dichroic spectra where the magnetic signal is given by the difference between the right and left circularly polarized signals. In Fig. 2(g)–2(j) we show X-ray resonant magnetic scattering (XRMS) and total electron yield (TEY) XMCD data as a function of the photon energy taken at the Mn and Cu L_3-absorption edge. A field of $H = -500$ Oe was applied in the plane of the sample along the [110] crystallographic direction at a temperature of 30 K. The induced Cu moment observed at the Cu L_3-edge is clearly observed. In contrast to absorption (TEY) spectroscopy, the reflectivity signal is also sensitive to dispersive parameters and necessitates modelling to extract absolute value for the magnetic moment of each LCMO layer. The signal was monitored while sweeping the magnetic field to record a hysteresis loop as shown in the bottom panel of Fig. 3.[73] It should be noted though, that the ratio of the steps in a multilayered sample can deviate from the expected values due to changes in the interference conditions with changes in the magnetic configuration.

The hysteresis loops with the field applied along [100] and [110] axes taken at the Mn L_3-edge highlight the different coercivities of both manganite layers. This probably results from a difference in the strain state, since during the growth of the YBCO layer the first LCMO layer will be fully strained while the top LCMO layer is (partially) strain relaxed. The larger coercivity and remanent magnetization along

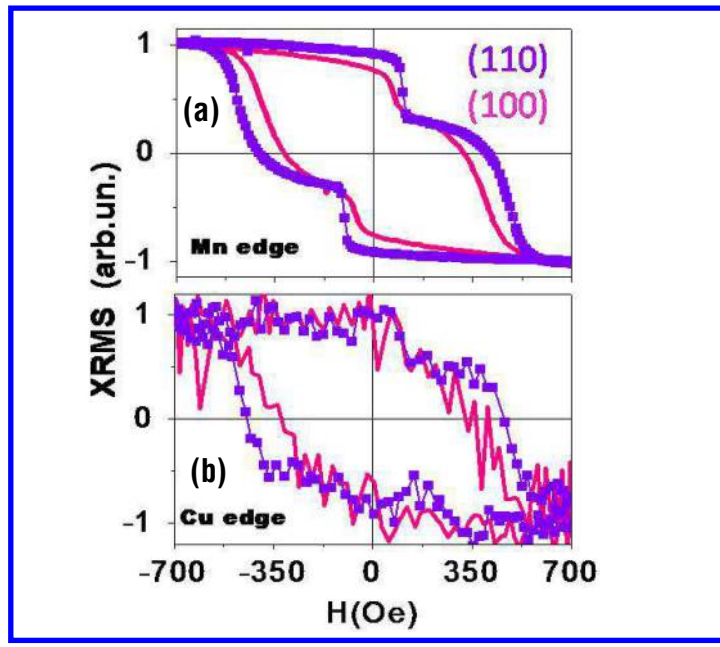

Fig. 3. (Color online) XMCD measurements performed at the Advanced Photon Source (Argonne National Laboratory) at beamline 4-ID-C X-ray magnetic reflectivity loops taken at L_3 Mn (a) and Cu (b) absorption edges at 30 K applying the field along [100] (red line) and [110] (black symbols). Figures adapted from Ref. 74.

the [110] direction is indicative of magnetic fields aligned with the easy axis.[74] Figure 3(b) shows the hysteretic behavior of the Cu magnetic moments through XMRS hysteresis loops. Cu and Mn loops display similar shape and coercivities: it becomes clear that the Cu moments switch follows closely the switching of the Mn moments. This is because the Cu magnetism results from the antiferromagnetic coupling to the interfacial Mn. Moreover, the fact that the magnetic response of Cu and Mn are similar indicates that the Cu at both interfaces is responding in the same proportion to Mn magnetic moments. Due to the surface sensitivity of the dichroism experiments, similar samples with thicker YBCO (12 nm and higher) showed only the Cu signal due to the top interface.

The symmetric interface reconstruction at both cuprate interfaces in LCMO/YBCO/LCMO structures evidences that there is a spin polarization induced at (both) interfacial Cu atoms, consistent with the symmetrical interface reconstruction. It is worth to mention here that other growth techniques, such as pulsed laser deposition, show different terminations at both interfaces.[75,76] Recent experiments in ultrathin cuprate layers with depressed (or suppressed) superconductivity in contact with manganites exhibit different temperature evolution depending on the existence or not of superconductivity.[77] The Cu magnetic state seems to survive up to higher temperatures in superconducting samples, indicating that the magnetic ground state is affected by the superconductivity. The interplay

between the interfacial magnetism and the mechanism of the high T_c superconductivity is an interesting question to pursue, which may provide important clues of the mechanism of the high T_c superconductivity itself.

As discussed below, the finding of Cu magnetism at both interfaces provide a firm footing for the applicability of recent models that explain the inverse superconducting spin switch behaviour of these trilayers in terms of the cancellation of the magnetic field associated with induced Cu moments by the applied field.

2.1. *Inverse superconducting spin switch*

The F/S/F trilayer system constitutes an experimental realization of the ferromagnetic superconducting proximity effect, which has attracted particular attention due to the possibility of amplified superconductivity modulation by controlling the relative magnetic alignment states of the F layers (parallel, P versus antiparallel, AP). The AP state has been proposed to average out the effect of the exchange field over the coherence volume resulting in large magnetoresistance ratios $((R_P - R_{AP})/R_P$ with $R_P > R_{AP})$ at a given temperature.[78–84]

In oxide-based $La_{0.7}Ca_{0.3}MnO_3$ (LCMO)/$YBa_2Cu_3O_7$ (YBCO)/$La_{0.7}Ca_{0.3}MnO_3$ (LCMO) trilayers,[85–91] quite contrarily, there is a different mechanism in which the T_c is reduced in the AP alignment.[92–94] Figures 4(a) and 4(b)

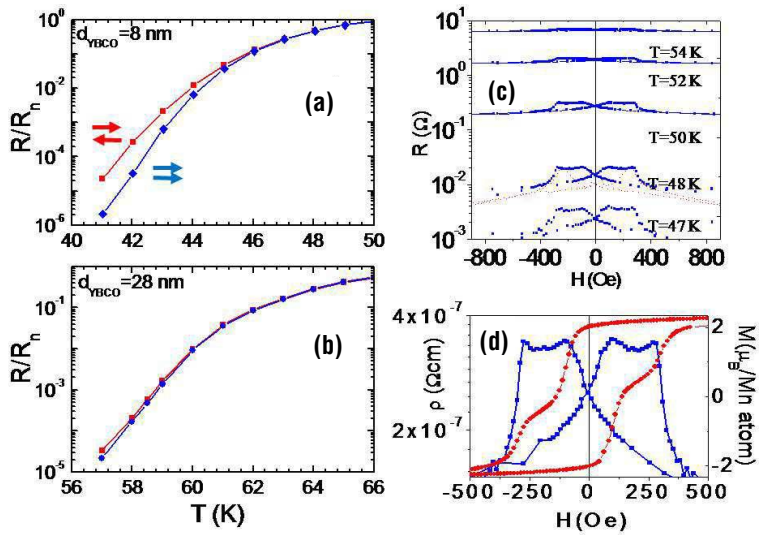

Fig. 4. (Color online) (a) Resistive transitions of LCMO/YBCO/LCMO trilayers with 15 nm LCMO layers and (a) thin (8 nm) and (b) thick (28 nm) YBCO layer. The red (blue) curves correspond to magnetization of the electrodes aligned parallel (antiparallel) to each other. (c) Magnetic field sweeps at selected temperatures along the transition yield a positive magnetoresistance plateaus which correspond to the increased resistance in the antiparallel configuration, as shown in panel (d). Notice that samples in a, b and c, d are different. Figures adapted from Refs. 88 and 90.

display resistive transitions of LCMO/YBCO/LCMO trilayers with 8 and 18 nm thick YBCO respectively measured with the current in plane geometry. In each panel the red and blue curves correspond to antiparallel and parallel alignment of the magnetization of the electrodes. Notice that resistance curves are shifted to higher temperatures in the parallel alignment, suggesting that superconductivity is favoured in this configuration. At a given temperature this yields a resistivity increase when the magnetic moments of the LCMO layers are aligned antiparallel. Figure 4(c) shows magnetic field sweeps at selected temperatures along the resistive transition. Notice that this yields *positive MR plateaus* for AP alignment of the magnetization of the F layers.

See Fig. 4(d) showing hysteresis loops together with magnetoresistance sweeps. The terms direct- and inverse superconducting spin switch have been introduced to describe enhanced (DSS) or depressed (ISS) superconductivity for antiparallel alignment of the magnetizations of the ferromagnetic layers. It has been accepted that an ISS governed by AP alignment ought to exhibit a well-defined *positive* plateau in the magnetoresistance (MR) between the two coercive fields of top and bottom layers,[82,83] while a DSS governed by the exchange field effect would have a *negative* MR plateau. Different explanations have been proposed to the ISS ranging from quasiparticle confinement in the S layer resulting from spin dependent scattering at the F/S interfaces to the effect of stray fields generated by domains or domain walls[95,96] in a way that in FSF structures may also be determined by magnetic alignment.[80,92,93] While all these effects depend on the relative alignment of the magnetizations of the ferromagnetic electrodes, recent experimental evidence obtained from detailed polarized neutron scattering experiments in rotating magnetic fields indicates that what matters is in fact the alignment of the magnetization to the applied magnetic field.[97]

Salafranca and Okamoto[98] have recently considered the anomalous proximity phenomena occurring at cuprate manganite interface from the perspective of competing interactions at the interfaces. The model considers a trilayer LCMO/YBCO/LCMO structure along the [001] direction. The pairing interaction in the cuprate involves the x^2–y^2 electrons. At the interface the $3z^2$–r^2 electrons of the cuprate become active due to the orbital reconstruction and hybridize with the e_g electrons of the manganite. This coupling is antiferromagnetic. The strong Hund coupling interaction of the cuprate couples the x^2–y^2 electrons to the $3z^2$–r^2 electrons ferromagnetically, and as a result the antiferromagnetic interaction at the interface is transmitted to the x^2–y^2 electrons. The model shows that as a result of the effective antiferromagnetic interaction of x^2–y^2 electrons to Mn core t_{2g} electrons there is an induced negative spin polarization at the cuprate, opposite to the positive spin polarization that one would expect in a spin injection scenario.[99] Induced spin polarization at the interface suppresses superconductivity. Superconductivity is completely suppressed when YBCO thickness is 2 unit cells in accordance with the experiment and survives (although with reduced T_c) up to a

thickness of 5 unit cells where bulk values are recovered. The length scale is set by the screening of the induced magnetization in the cuprate which occurs within 2 to 3 unit cells from the interface in absence of superconductivity. This is an important theoretical result which shows that the induced magnetization in the Cu lattice is not restricted to the interface plane as one would guess from a pure orbital picture, but it extends into the cuprate with a short length scale determined by the hopping rate in the z direction. In presence of superconductivity interface magnetization is reduced and screening becomes oscillatory up to a thickness of 4 to 5 unit cells from the interface where induced spin polarization vanishes. This model correctly captures the long length scale of the anomalous proximity effect of 8 to 10 unit cells observed in trilayers and superlattices where superconductivity is being suppressed at the two interfaces of the cuprate layer.

The inverse superconducting spin switch effect is also correctly accounted for by Okamoto and Salafranca's model. Looking now at the effect of an applied magnetic field on a trilayer system, the key idea is how the externally applied magnetic field (parallel to the layers) competes with the exchange field of the induced spin polarization of the cuprate. Right at the interface this exchange field may be very large (~ 100 T), but it decays exponentially away from it. For parallel alignment of the manganite moments, the applied magnetic field compensates the exponential tail of the exchange field due to the Cu spin polarization. This gives rise to a recovery of T_c in this region. For antiparallel alignment of the magnetic moments of the electrodes the system is symmetric against an inversion of H and although there may be a compensation of the exchange field at one interface there will add up at the other. The T_c recovery in the parallel configuration due to the compensation of the Cu exchange field, which does not occur in the antiparallel configuration, is the reason underlying the inverse superconducting spin switch which seems to favor superconductivity in the parallel configuration. This also explains the positive magnetoresistance peaks (plateaus) observed in isothermal resistance versus magnetic field sweeps when the manganite layers are antiferromagnetically aligned. At a given temperature, enhancement of T_c in the parallel configuration is responsible for a lower resistance level as compared to the antiferromagnetic configuration.

3. Ti Magnetism at Titanate Manganite Interfaces

In this section we examine interfacial Ti magnetism in heterostructures combining manganites and titanates. The Mn-O-Ti superexchange path at the interface splits the Ti band and induces a magnetic moment which is detected by XMCD. Controlling epitaxial strain allows changing the orbital occupancy at the interface what provides a path to control orbital reconstruction and magnetic interaction.

3.1. *$LaMnO_3/SrTiO_3$ interface*

Let us start with the $LaMnO_3/SrTiO_3$ (LMO/STO) heteroepitaxy, a system with a variety of interesting ingredients. Despite their common perovskite structures

there is substantial epitaxial mismatch strain which may play a role in stabilizing distortions and rotations of the oxygen octahedra. For [001] growth there is also a polarity mismatch at the interface similar to that found in the LAO/STO system (LMO planes are polar while STO planes are nonpolar), and similar physics might be at play. Moreover, both materials are also electronically very different. In $LaMnO_3$, Mn^{3+} ion has a d^4 electronic configuration, the t_{2g} band is fully occupied and there is a single electron in the e_g levels. In its bulk form the strong crystal field and electron–lattice (JT) interactions lift orbital degeneracy giving rise to an in-plane ordering of the e_g orbitals which yields the A type antiferromagnetic states, where Mn ions couple ferromagnetically in plane while neighboring planes are antiferromagnetically coupled. In titanates with a trivalent A site element, such as $LaTiO_3$, Ti^{3+} is in a d^1 state and thus the t_{2g} band is singly occupied. The small overlap of t_{2g} orbitals, mediated by weak O π bonds which are not directed along [100] bond directions, give rise to the small crystal field splitting and the weak JT coupling as compared to manganites with e_g orbitals. Owing to the nearly cubic environment of the Ti ions, they exhibit a larger tendency to orbital degeneracy and may thus display orbital moments and low temperature ferromagnetism. However, there are important open questions such as the lack (or very small values) of the orbital moment[100–103] or the experimental absence of the theoretically predicted ferromagnetism for $LaTiO_3$,[42,104] whose importance at our interfaces will become clear later.

Samples were $[LMO_M/\ STO_N]_8$ superlattices consisting of 8 periods of M unit cells of LMO and N unit cells of STO grown by high pressure oxygen sputtering.[105,106] M ranged from 3 to 17 and N from 2 to 12 unit cells. Interfaces were sharp as identified by X-ray diffraction [Fig. 5(a)] and STEM images (Fig. 5(b)]. X-ray absorption and electron energy loss spectroscopy (EELS) with atomic column resolution indicate the presence of Ti^{3+} ions in the STO layers.[105,106] These electrons reside in the t_{2g} orbitals of a Ti band at the interfacial plane which essentially behaves as an "artificially doped" interfacial titanate. In other words, due to the existence of a LaO termination plane the interface behaves as a $LaTiO_3$ unit cell thick layer. The interfacial MnO_2 plane has an oxidation state close to 3+ (from EELS) with the $3t_{2g}$ levels half-filled (due to Hund coupling) and one electron occupying the e_g band. There is also hole doping in the manganite layers characteristic of LMO in thin film form. Thin film LMO usually displays a ferromagnetic insulating ground state resulting from unintentional hole doping associated stoichiometry imbalances. The transport and magnetic properties are controlled by epitaxial strain through its dependence on the thickness ratio. For a given thickness of the titanate layer of 2 unit cells, the thickness of the manganite layer controls epitaxial strain: In the following we will focus on experiments on samples exhibiting two extreme behaviors. One is a sample with 17 unit cell thick LMO and 2 unit cells of STO [LMO 17/STO 2], and the other has 3 unit cells of LMO and 2 unit cells of STO [LMO 3/STO 2]. For very thin manganite in a 3/2 superlattice, structure matches the STO in plane lattice parameters while for 17/2 superlattices with thick relaxed

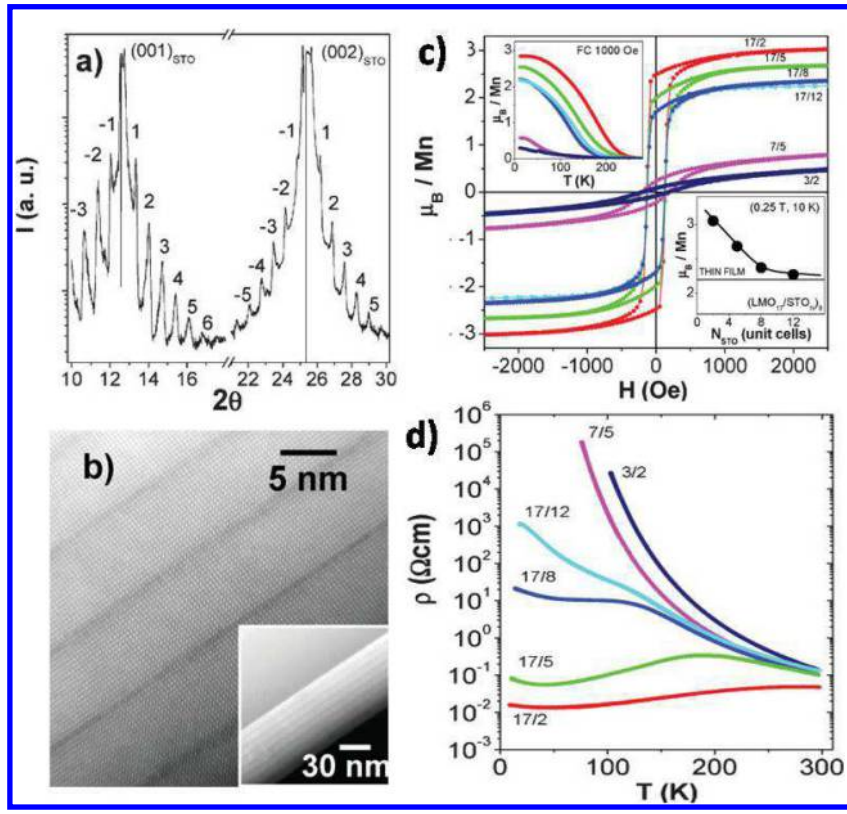

Fig. 5. (Color online) (a) High angle θ–2θ X-ray spectra of the $(LMO_{17}/STO_2)_8$ superlattice. The data has been acquired with synchrotron radiation of wavelength 0.855 Å. The superlattice satellite peaks are indexed. (b) High and low (inset) magnification Z-contrast images of the same sample. (c) Hysteresis loops of the samples measured at 10 K. The N/M labels correspond to the LMO/STO layers thickness in unit cells of each sample. Top inset: FC magnetization versus temperature with an applied magnetic field of 1000 Oe of the same samples. The different samples have been coloured, and the colour code is preserved through the figure. Bottom inset: Magnetization versus STO thickness of the $(LMO_{17}/STO_n)_8$ series measured at 10 K and 0.25 T. The line represents the magnetization of the 22 unit cells LMO thin film measured under the same conditions. (d) Logarithmic resistivity curves of the same samples. The same label nomenclature and color code has been used in both panels. Figures adapted from Ref. 105.

manganite layers, the crystalline lattice matches the manganite in plane lattice parameters. While the 3/2 superlattices clamped to the STO substrate are insulating and weakly ferromagnetic, the relaxed 17/2 superlattices display the full magnetic moment and a metallic ground state (see Fig. 5).

The electron-doped STO layers possess a magnetic moment as clearly indicated by the presence of a strong XMCD signal [see Fig. 6(a)]. Figures 6(a) and 6(b) show XMCD spectra measured at the Ti and Mn edges, respectively. Figure 6(b) shows that there is a magnetic spin moment at the Mn edges in both samples, demonstrating that both samples are magnetic, as confirmed by magnetometry. Figures 6(c) and 6(d) display the integrated area under the XMCD spectra for Ti

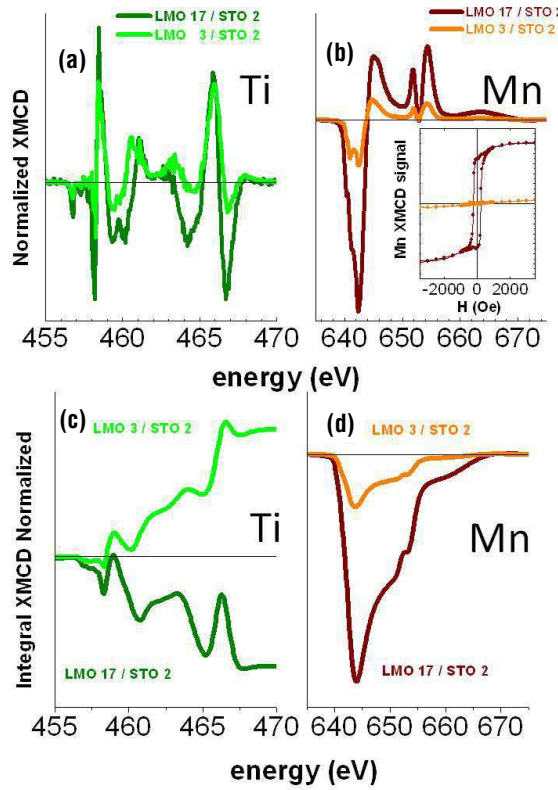

Fig. 6. (Color online) Ti (a) and Mn (b) normalized XMCD spectra of the [LMO 3/STO 2] and [LMO 17/STO 2] superlattices measured at 6 K. The XMCD measurements are normalized to the L_3 t_{2g} (Ti) and L_3 (Mn) edge jump values. Inset: Mn hysteresis loops of the same samples obtained from Mn XMCD signal. Integrated values of the Ti (c) and Mn (d) normalized XMCD spectra of the [LMO 17/STO 2] and [LMO 3/STO 2] superlattices. Figures adapted from Ref. 106.

(c) and Mn (d) edges, which is directly proportional to the orbital moment. Interestingly, while the integrals of the Mn XMCD spectra show that the orbital moment is essentially quenched as expected, there is a significant orbital component to the magnetic moment of the Ti [see Fig. 6(c)]. The shape of the XMCD signal of both the Mn and Ti [see Figs. 6(a) and 6(b)] depends strongly on the thickness ratio of the superlattices. Notice that both samples display opposite signs of the integrated intensity under the Ti XMCD signal [see Fig. 6(c)], clearly indicating a change in the coupling mechanism of the Ti and Mn spin moments at the interface. Note that the value of the Ti spin moment estimated from the application of the sum rules (0.2 μ_B/Ti for the [LMO 3/STO 2] and 0.15 μ_B/Ti for the [LMO 17/STO 2]) are to great extent underestimated. Furthermore, the temperature dependence of the Ti moment closely follows that of the Mn moment, and essentially vanishes at the Curie temperature of the manganite suggesting that the Mn–O–Ti superexchange is responsible for the Ti ferromagnetism in this sample.

The plots of the integrals of the XMCD signals indicate that the orbital and spin moments of the Ti 3*d* electrons are aligned antiparallel according to 3rd Hund's rule, evidencing the effect of spin orbit interaction. Spin-orbit coupling is a mechanism by which spins feel the distribution of the electronic density (orbits) and contrary to e_g systems, the matrix elements of the orbital momentum operator acting on t_{2g} states are nonzero (though small, typically spin orbit interaction is ~ 20 meV for titanates).[2] The unambiguous presence of an orbital moment anti-aligned to the spin, constitutes direct evidence that the orbital degeneracy is not completely lifted (which would result in a complete quenching of the orbital moment). It is worthwhile recalling that experimental evidence in bulk LTO suggests that the orbital moment is almost completely quenched and no evidence of orbital magnetism has been found so far,[103] making this finding even more surprising and unexpected.

The change of the sign of the coupling interaction between Mn and Ti spin moments from antiferromagnetic in the 17/2 to ferromagnetic in the 3/2 superlattice can be explained in terms of changes in the orbital polarization of the interface resulting from the different strain states.[107] In the 17/2 superlattice there is preferential occupation of Mn $3z^2$–r^2 band at the interface, while in the strained 3/2 superlattice Mn x^2–y^2 are preferentially occupied.[106,107] Semicovalent bonds at the interface result from the hybridization of $3z^2$–r^2 and t_{2g} xz and yz active orbitals (both spin up and spin down). It can be observed in Fig. 7(a) that in the [LMO 17/STO 2] superlattice there is strong hybridization between the preferentially occupied Mn $3z^2$–r^2 band at the interface and the empty $3z^2$–r^2 band of Ti. The occupation of the hybridized orbitals at the interface explains the AF alignment of the Ti moment with respect to the Mn moment.[99] Three of the electrons of the Mn occupy the spin up $3z^2$–r^2 and the active t_{2g} xz and yz hybrids, while the fourth occupies an inactive t_{2g} xy orbital which does not participate in bonding. The Ti t_{2g} electron occupies the spin down t_{2g} hybrid, and thus its alignment is antiferromagnetic [see Fig. 6(d)]. The dominant superexchange process occurs between the Ti t_{2g} electrons and the half-filled Mn t_{2g} bands and, according to Goodenough–Kanamori rules, is antiferromagnetic. In the [LMO 3/STO 2] super-

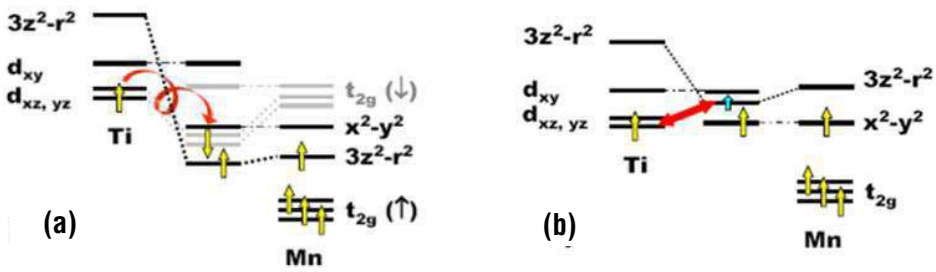

Fig. 7. (Color online) Schematic energy diagrams of the orbital hybrids proposed for LMO/STO interfaces as a function of Mn orbital polarization: (a) Preferential Mn $3z^2$–r^2 orbital occupation and (b) Preferential Mn x^2–y^2 orbital occupation. (Adapted from Ref. 106.)

lattices the occupation of the Mn x^2–y^2 orbitals at the interface identified by XMLD changes the hybridization pattern.[106] The hybridization between the occupied Mn x^2–y^2 and Ti orbitals across the interface is negligibly small. A finite overlap between Ti t_{2g} and Mn $3z^2$–r^2 orbitals resulting from the $GdFeO_3$-type distortion of the manganite may yield finite values of the transfer integral between $3z^2$–r^2 and t_{2g} active orbitals xz and yz. Ferromagnetic coupling in [LMO 3/STO 2] results from the superexchange interaction through the virtual excitation of electrons from Ti xz, yz to Mn $3z^2$–r^2 [see Fig. 7(b)]. This simple molecular orbital picture, with mean-field type treatment for the interaction, provides a simple explanation for the magnetic coupling of Ti and Mn moments at the interface. At this stage we cannot make a definitive statement on the importance of corrections due to many-body effects or more complex spin-orbital superexchange processes not considered here.

The experiments on LMO/STO heterointerfaces between an electron-doped titanate and a manganite show evidence for Ti spin and orbital magnetism. The orbital magnetic moment requires the presence of a small splitting between t_{2g} levels. This result constitutes a practical realization of orbital magnetism at an interfacial titanate layer which is not found in bulk titanates. Depending on the strain state of the superlattice, controlled by the manganite-to-titanate thickness ratio, the sign of the spin–spin coupling at the interface is reversed, outlining the role played by the orbital reconstruction at the interface in tailoring exchange interactions. This novel form of interface magnetism will provide important clues for the understanding of the effects of orbital degeneracy in superexchange

3.2. $La_{0.7}Sr_{0.3}MnO_3$ /$SrTiO_3$ interface

The finding of induced magnetism at the interface between the Mott insulator $LaMnO_3$ and the band insulator $SrTiO_3$[105,106] has motivated further studies in the technologically more relevant $La_{0.7}Sr_{0.3}MnO_3$ (LSMO)/$SrTiO_3$(STO) interface.[108] Interfacial magnetism may have important practical implications in the operation of magnetic tunnel junctions where spin polarization of the injected current may be influenced by the spin structure at the interface. Among correlated electron systems, LSMO has been extensively studied as a possible source of spin polarized electrons at room temperature.[109] The large values of tunnelling magnetoresistance (TMR) reported for LSMO/STO/LSMO tunnel junctions at low temperature drops way below the Curie temperature of the magnetic electrodes, suggesting that a depolarisation of the injected current may occur at the interface.[110] This effect has been attributed to deteriorated magnetic properties of the manganite layer at the interface, a so called "dead layer" whose origin is still not well understood.[111,112] When the magnetic structure of the interface is examined in the light of its modified orbital structure, a magnetic moment induced at the Ti is also found which results from the orbital reconstruction. Charge leaks into the otherwise empty t_{2g} orbitals of the titanate which, as a result of the hybridization with Mn orbitals, become magnetic. This is fundamentally different from previous reports of interfacial

magnetism like the case of Cu[45] or Fe[119] where the interfacial magnetism is a consequence of a reordering of pre-existing moments. In our case, Ti atoms, nominally in a 4+ state, have no magnetic moment in absence of electronic reconstruction.

In the following results are described corresponding to two series of $[LSMO_6/STO_2]_8$ superlattices consisting of 8 bilayers of 6 LSMO unit cells (u.c.) and 2 STO u.c., grown on (100) STO substrates using a high-pressure pure oxygen sputtering technique. The Ti oxidation state examined by atomic column resolution EELS has been shown to evolve from $Ti^{3.75+}$ when STO is 2 u.c. thick to Ti^{4+} when STO is 8 u.c. thick. While Ti atoms at the bulk of the layer are in a 4+ oxidation state when bilayer index (and STO layer thickness) increases, the interfacial Ti seems to exhibit a reduced oxidation state according to the EELS maps. The Mn oxidation state, on the other hand, remains constant and close to the 3.3+ expected for the nominal stoichiometry. The reduced oxidation state found for the Ti in the ultrathin STO layers most likely result from an electronic reconstruction at the manganite-titanate interface. La–Sr intermixing could also cause the reduced oxidation state of Ti. However, if electron doping of STO were caused by La enrichment this would imply a hole enrichment of the LSMO near the interface, which in fact is not observed.

XMCD experiments were also performed on superlattices with different STO thicknesses. Figure 8(a) shows XMCD spectra taken at the Mn and Ti L edge of a $[LSMO_6/STO_2]_8$ sample measured at 6 K and with an applied field of 10 kOe. A clear dichroic signal is also observed at the Ti edge demonstrating the induced magnetism at the STO, a remarkable result considering that bulk STO is a diamagnetic band insulator. The temperature dependence of the XMCD signal shown on Fig. 8(b) evidences that the Ti (466 eV) XMCD signal closely follows Mn (642 eV) signal and magnetization. The magnitude of the Ti signal scales with the magnitude of the Mn signal, demonstrating that the origin of the Ti moment is the interaction with the Mn moment. A rough estimate of the magnitude of the magnetic moment of Ti $M_s = -0.04\ \mu_B/at_{Ti}$ was obtained by applying sum rules.[113] The negative value of the Ti moment indicates that its direction is opposite to the magnetic field, and hence that the Mn–Ti coupling is antiferromagnetic.

An explanation for the antiferromagnetic Mn–Ti coupling at the interface can be offered in terms of the modified bonding at the interface in the same line as we did in the case of the LMO/STO system. Since t_{2g} orbitals in STO are located slightly above the Fermi level of the manganite, orbital hybridization may drive an electronic reconstruction at this interface.[7] In particular we propose a scenario where hybridized "down" xz, yz bonding orbitals reside lower in energy than hybridized "up" bonding $3z^2$–r^2 orbital, thus yielding the antiferromagnetic Ti state. This hybridized-orbital picture is a natural consequence of the lattice mismatch between STO and LSMO and the reduced electron density in LSMO compared with undoped $LaMnO_3$. The former increases the energy level of the bonding $3z^2$–r^2 orbital, and the latter suppresses the occupation of the bonding $3z^2$–r^2 orbital. These effects

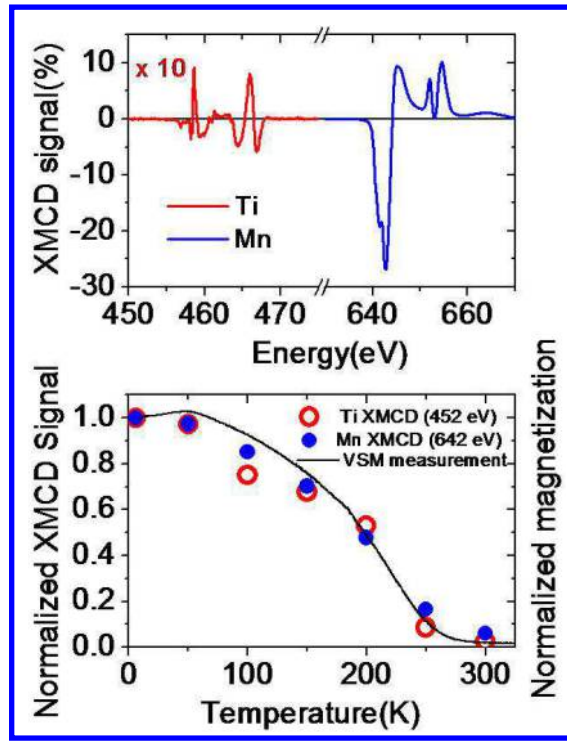

Fig. 8. (Color online) XMCD measurements performed in a $[LMSO_6/STO_2]_8$ superlattice. (a) XMCD signals obtained from the Ti $L_{2,3}$ edge (red) Mn $L_{2,3}$ edge (blue). Ti signal has been multiplied by a factor of 10. (b) Temperature dependence of the XMCD signal. Ti (red open circles) and Mn (blue solid circles) XMCD signal taken at 452 eV and 642 eV, respectively and VSM measurement (black line), all measurements are normalized to the value at 4 K. Figures adapted from Ref. 108.

cooperatively destabilize the ferromagnetic coupling via either the double-exchange or superexchange interaction mediated by the $3z^2$–r^2 orbital as discussed by Garcia-Barriocanal *et al.*[105,106] Because of the charge transfer occurring at this interface and electron doping by $La_{0.7}Sr_{0.3}O$ layer, Ti is in a mixed 3+/4+ oxidation state at the interface, resulting in the antiferromagnetic coupling with respect to Mn. The destabilization of the out of plane ferromagnetic interaction in the manganite may be the origin of a stronger decrease of the ordered moment than in the bulk when temperature is increased.[99] This effect might account for the rapid suppression of the tunnelling magnetoresistance of LSMO/STO magnetic tunnel junctions when temperature is increased.

A related interesting scenario is the induced Ti magnetism in $La_{0.7}Sr_{0.3}MnO_3$/$BaTiO_3$/Fe magnetic tunnel junctions.[114] The charge redistribution theoretically predicted at Fe/$BaTiO_3$ interfaces may modify the spin polarization at the interface depending on the direction of the ferroelectric polarization of the $BaTiO_3$ layer, and be the source of interesting magnetoelectric coupling effects.[115–118] Recipro-

cally, it has been recently shown that there is magnetism induced at the Ti edge at the BTO/Fe interface suggesting a new path towards artificially designed multiferroics. Evidence of a Ti ferromagnetic state has been obtained from X-ray resonant magnetic scattering hysteresis loops at Ti $L_{2,3}$ and O K edges. Combined interface imaging by aberration corrected STEM EELS and modeling suggests that in this case Ti is in a 4+ state. Ti atoms are spin polarized due to the hybridization with Fe and spin polarized oxygen atoms suggesting that the mechanism at play may be different from that outlined previously in manganite/titanate heterojuctions.

4. Magnetism at Manganite Ferrite $La_{0.7}Sr_{0.3}MnO_3/BiFeO_3$ Interfaces

Induced magnetism at $La_{0.7}Sr_{0.3}MnO_3/BaFeO_3$ (LSMO/BFO) interfaces has been recently examined by Ramesh's group.[119] This is an interesting case where the BFO is a multiferroic with an antiferromagnetic groundstate. The superexchange interaction with the ferromagnetic manganese at the interface induces a canting in the antiferromagnetic lattice of Fe moments. A new phenomenology shows up in this system due to the effect of orbital reconstruction in lifting the e_g degeneracy, what causes a change in the magnetic interaction at the interface. I.e., the strong orbital hybridization in the growth direction originates a x^2–y^2 orbital polarization at the interface which destabilizes the ferromagnetic interaction along the z direction. As a result, the interfacial Mn may change its intra plane and interplane coupling to the next Mn in the second layer, giving rise to an interface Mn layer with modified magnetic properties coupled AF to the second Mn layers. The resulting interfacial magnetic coupling is thus controlled by the orbital reconstruction at the interface.

In this system, Fe in a 3+ oxidation state is in a d^5 electronic state such that charge transfer is prohibited due to the ground state electronic structure of the transition metal at the interface. Contrary to the case of the cuprate interface where the (unpolarized) x^2–y^2 level lies just above the Mott gap allowing the charge transfer process, in the case of Fe^{3+} in a high spin state the down spin x^2–y^2 state is located far above the gap, and thus charge transfer is not allowed. At this interface with a multivalent Mn (3+/4+) transition metal ion, a modification of the magnetic ground state of the manganite occurs. The proposed bond reconstruction at the interface is as follows. It is assumed that the e_g energy levels of the BFO lie lower in energy than those of LSMO. There is a strong hybridization between $3z^2$–r^2 orbitals to form a $3z^2$–r^2 bonding state, lower in energy, and a $3z^2$–r^2 antibonding state, higher in energy. x^2–y^2 orbitals will not be influenced because their symmetry does not allow hybridization at (001) interfaces. The lowest electronic states, occupied by bond reconstruction will be the hybrid $3z^2$–r^2 bonding states and the Mn x^2–y^2 nonhybridizing states. According to the Goodenough-Kanamori rule,[38,39] the superexchange coupling between Fe^{3+} and Mn^{3+} (with in plane x^2–y^2 orbital ordering) or Mn^{4+} is expected to be strongly ferromagnetic. On the other hand the interfacial Mn layer with modified x^2–y^2 orbital ordering naturally leads to the anti-

ferromagnetic coupling with its neighboring Mn layer. As a result the interfacial Fe spins and the Mn spins in the bulk LSMO region are coupled antiferromagnetically.

This behavior suggests the possibility of exploiting the competition between ground states with similar characteristic energies which can be preferentially stabilized due to changes in the bond or orbital symmetry occurring at the interfaces.

5. Magnetism at the $LaAlO_3/SrTiO_3$ Interface

The finding of a conducting interface between two band insulators in $LaAlO_3$ and $SrTiO_3$ bilayer by Ohtomo and Hwang[8,9] has generated a tremendous scientific interest. The interfacial conductivity has been proposed to originate at a charge transfer process from the surface of the LAO down to the interface to avoid the polar catastrophe,[11,12] namely the unlimited growth of the electrostatic energy which would result from the polar nature of the (001) planes of the LAO. Due to the built up electric field band bending (tilting) occurs, and above a thickness of 3 to 4 unit cells of LAO the valence band edge of the LAO reaches the Fermi level allowing the charge transfer process. Other explanations in terms of extrinsic effects such as oxygen vacancies[12–15] or cation diffusion[16–18] and structural distortion or orbital reconstruction[120] have also been proposed. The tunability of the interfacial carrier density by using a gate voltage has allowed exploring a wide variety of phenomena which appear to compete at this interface, including superconductivity,[21] magnetism,[22] and their coexistence.[121,123,124] While the superconductivity of doped STO has been known for years important open questions regard the nature and origin (extrinsic or intrinsic) of the magnetic state of the STO and whether or not the coexistence with superconductivity is an exotic ground state of the correlated electron liquid at the interface. The coexistence of both orders inferred from hysteretic magnetoresistance in doped STO layers and interfaces have led to the conclusion that band filling and Coulomb repulsion may indeed play a role, and a carrier controlled mechanism has been proposed.[125] The first reports of magnetism by Brinkman and colleagues[22] were based on low temperature hysteretic magnetoresistance of LAO/STO samples prepared at high oxygen pressures to ensure a low carrier density. However, recently, room temperature ferromagnetism was claimed by Ariando for 10 unit cells of $LaAlO_3$ on $SrTiO_3$ in fields up to 0.2 T based on SQUID magnetometry.[122] Li *et al.*,[123] based on torque magnetometry measurements reported moments of 5 10^{-10} Am^2 for an ultrathin 5 unit cells thick layer of $LaAlO_3$ on $SrTiO_3$. Finally, Bert *et al.*,,[124] using a scanning Hall probe contact microscopy have found evidence of micron size magnetic patches with a large associated dipole field consistent with magnetism generated by localized carriers. On the other hand, neutron scattering experiments on LAO/STO superlattices with conducting and nonconducting interfaces do not detect the signature of a ferromagnetic interface state.[126] It is known that polarized neutron reflectometry is well suited to explore magnetism at surfaces or interfaces, and in particular, the spin asymmetry is very sensitive to small magnetization values. The spin asymmetry,

the difference between integrated intensities under a Bragg peak for magnetic fields applied parallel or anti parallel to the spin polarization of the neutron beam, is extremely sensitive to interface magnetism, while the spin asymmetry at the critical angle probes the magnetization averaged over the entire superlattice. No significant spin difference was measured near the critical edge of the $LaAlO_3/SrTiO_3$ superlattice. On the other hand, by measuring the spin asymmetry under the first Bragg peak established an upper limit of 2 G for the magnetization change across the $LaAlO_3/SrTiO_3$interfaces (laterally averaged) at 11 T and 1.7 K. If attributed to Ti, the 2 G upper limit for the magnetic moment would correspond to 0.7% of Ti^{3+} per unit cell. If averaged over the entire superlattice this magnetization is likely to be less than the upper limit of 1 G inferred from measurement of substrate control experiments. In summary, the upper level of 2 G found[126] using a technique well suited to probe interface magnetism questions the intrinsic origin of the magnetism ascribed to the LAO/STO interfaces.

6. Summary and Outlook

We have described a class of low dimensional magnetism appearing at the interface between magnetic and nonmagnetic oxides. It originates at the new superexchange path occurring at the bonding discontinuity at the interface, and traces a new route to induce magnetism in the otherwise nonmagnetic material. The phenomenon is quite ubiquitous, and has been observed experimentally at interfaces involving manganites,[45,46,105,106,108] ferrites[119] and nickelates.[127] Its origin is the splitting of its bands due to the hybridization with the exchange split bands of the magnetic material. The sign of the magnetic coupling between the magnetic and the nonmagnetic elements forming the reconstructed bond can be controlled by external variables such as charge transfer and epitaxial strain through their effect on orbital symmetry and filling. The ability to tune this magnetic state[128,129] is of utmost importance since it opens the possibility of controlling the induced magnetism by external parameters such as electric polarization or electric field. The strong electric fields at the interfaces with tunnel barriers may induce charge transfer processes and thus modify band filling. Furthermore, it may modify the relative energy position of the energy levels corresponding to the materials building an interface, especially if charge depleted (space charge) regions occur as a result of differences in the electrochemical potential. These space charge regions can be very narrow, of the width comparable to one unit cell, at junctions between a metal and a Mott insulating barrier. A very large electric field may thus develop in a narrow region at the interfaces which may change the energy separation between levels of both materials, allowing for changes in the orbital reconstruction. Of particular interest is to explore induced magnetism at interfaces with ferroelectric materials.[130–134] At interfaces with ferroelectrics, the reversal of the polarization, aside from changes in the carrier density occurring to screen the polarization charges,[135] may cause changes in the hybridization at the interface resulting from the lattice distortions

associated to the polarization states. This may allow for charge transfer processes or level splitting which may profoundly modify the induced magnetic moments at the interface, as it has been recently theoretically shown.[115–118] The possibility of modifying the magnetic ground state of interfaces with the polarization states may be an interesting pathway towards electric field control of magnetism.

Another interesting direction is to exploit the tendency of correlated oxides to phase separation to stabilize at interfaces electronic ground states with specific (magnetic) functionalities. This is the case of the electronic reconstruction occurring at the interface between two manganese perovskite oxides, one being ferromagnetic-metallic ($La_{0.7}Ca_{0.3}MnO_3$) and the other antiferromagnetic-insulating ($La_{0.3}Ca_{0.7}MnO_3$).[136] As a result, an insulating phase with a significant interface-induced magnetic moment is stabilized at the interface. This phase, which according to the bulk phase diagram is not expected, is functionalized as an active barrier in magnetic tunnel junctions and mimics a spin-filtering behavior. At manganite interfaces and surfaces, electronic phases different from those of the bulk compounds may be stabilized as a consequence of a subtle competition between the kinetic energy (that favor ferromagnetism) and the localizing interactions (which favor antiferromagnetism and insulating behavior). The ground state properties of manganites are determined by the competition between at least four independent energy scales: the antiferromagnetic (AF) interaction between the Mn spins, the electron phonon coupling, the electronic repulsion, and the kinetic energy of the carriers. In manganites, the energies involved in these interactions are comparable so very different states can have very similar energies. Consequently, by slightly varying parameters such as carrier concentration, strain, disorder, or temperature, different ground states can be experimentally observed. Extending this approach to antiferromagnetic oxides with high ordering temperature should expand dramatically the range of simple spin-filter materials and inspire novel concepts in oxide spintronics. This may constitute a promising route towards novel magnetoelectric effects to manipulate spin-polarized currents, and to circumvent the scarcity of spin-filter materials, offering new opportunities in spintronics.

In summary, interfacially induced magnetism occurring at interfaces between correlated oxides could find interesting functionalities in devices with operation controlled by the interface such as tunnel or field effect devices. In particular magnetic interfacially induced states in Mott insulating barriers could be useful to modify the spin polarization of injected currents or have spin selective transport yielding interesting novel spin filtering functionalities of interest in spintronics.

Acknowledgments

We want to thank Maria Varela and Steve Pennycook of the STEM Group at the Electron Microscopy at the Materials Science & Technology Division at Oak Ridge National Laboratory for performing the electron microscopy and spectroscopy structures. Suzanne te Velthuis, Yaohua Liu and Axel Hoffmann of the Materi-

als Science Division, Argonne National Laboratory and Mike Fitzsimmons from Los Alamos National Laboratory for polarized neutron reflectometry experiments and collaboration and discussion. Agnes Barthelemy and Manuel Bibes from Unité Mixte de Physique CNRS/Thales for steady collaboration and discussions. The theory support and stimulating discussions with Satoshi Okamoto are also acknowledged. We acknowledge financial support by Spanish MICINN through grants MAT2011-27470-C02 and Consolider Ingenio 2010 CSD2009-00013 (Imagine), by CAM through grant S2009/MAT-1756 (PHAMA).

References

1. M. Imada, A. Fujimori and Y. Tokura, *Rev. Mod. Phys.* **70**, 1039 (1998).
2. S. Maekawa *et al.*, in *Physics of Transition Metal Oxides* (Springer, 2004), Chap. 1.
3. E. Dagotto, *Science* **309**, 257 (2005).
4. E. Dagotto and Y. Tokura, *MRS Bull.* **33**, 1037 (2008).
5. J. Mannhart and D. G. Schlom, *Science* **327**, 1607 (2010).
6. H. Y. Hwang, *Nat. Mater.* **11**, 103 (2012).
7. S. Okamoto and A. Millis, *Nature* **428**, 630 (2004).
8. A. Ohtomo *et al.*, *Nature* **419**, 378 (2002).
9. A. Ohtomo and H. Hwang, *Nature* **427**, 423 (2004).
10. N. Nakagawa, H. Y. Hwang and D. A. Muller, *Nat. Mater.* **5**, 204 (2006).
11. For a review see, J. N. Eckstein, *Nature* **6**, 473 (2007).
12. K. Yoshimatsu *et al.*, *Phys. Rev. Lett.* **101**, 026802 (2008).
13. S. A. Chambers, *Phys. Rev. Lett.* **102**, 199703 (2009).
14. K. Yoshimatsu *et al.*, *Phys. Rev. Lett.* **102**, (2009) 199704.
15. A. Kalabukhov *et al.*, *Phys. Rev. B* **75**, 121404(R) (2007).
16. P. R. Willmott *et al.*, *Phys. Rev. Lett.* **99**, 155502 (2007).
17. A. S. Kalabukhov *et al.*, *Phys. Rev. Lett.* **103**, 146101 (2009).
18. A. Kalabukhov *et al.*, *Europhys. Lett.* **93**, 37001 (2011).
19. S. Thiel *et al.*, *Science* **313**, 1942 (2006).
20. A. D. Caviglia *et al.*, *Nature* **456**, 624 (2008).
21. N. Reyren *et al.*, *Science* **317**, 1196 (2007).
22. A. Brinkman *et al.*, *Nat. Mater.* **6**, 493 (2007).
23. M. Baibich *et al.*, *Phys. Rev. Lett.* **61**, 2472 (1988).
24. M. C. Cyrille *et al.*, *Phys. Rev. B* **62**, 15079 (2000).
25. M. C. Cyrille *et al.*, *Phys. Rev. B* **62**, 3361 (2000).
26. J. Santamaria *et al.*, *Phys. Rev. B* **65**, 012412 (2002).
27. J. Santamaria *et al.*, *Phys. Rev. Lett.* **89**, 190601 (2002).
28. M. E. Gomez *et al.*, *Eur. Phys. J. B* **30**, 17 (2002).
29. M. E. Gomez *et al.*, *Phys. Rev. B* **71**, 125410 (2005).
30. A. Scherz, H. Wende and K. Baberschke, *Appl. Phys. A* **78**, 843 (2004).
31. H. Wende *et al.*, *J. Phys.: Condens. Matter* **15**, S547.
32. F. Wilhelm *et al.*, *Phys. Rev. Lett.* **87**, 207202 (2001).
33. R. Tyer *et al.*, *Phys. Rev. B* **67**, 104409 (2003)
34. R. Coehoorn, *J. Magn. Magn. Mater.* **151**, 341 (1995).
35. E. R. Moog, J. Zak and S. D. Bader, *J. Appl. Phys.* **69**, 4559 (1991).
36. N. Nakajima *et al.*, *Phys. Rev. Lett.* **81**, 5229 (1998).
37. R. Wu, C. Li and A. J. Freeman, *J. Magn. Magn. Mater.* **81**, 71 (1991).
38. J. B. Goodenough, *Phys. Rev. B* **100**, 564 (1955).

39. J. Kanamori, *J. Phys. Chem. Solids* **10**, 87 (1959).
40. Y. Tokura and N. Nagaosa, *Science* **288**, 462 (2000).
41. J. Garcia-Barriocanal *et al.*, *Science* **321**, 678 (2008).
42. T. Mizokawa, D. I. Khomskii and G. Sawatzky, *Phys. Rev. B* **60**, 7309 (1999).
43. J. Stöhr, *J. Magn. Magn. Mater.* **200**, 470 (1999).
44. H. Wende, *Rep. Prog. Phys.* **67**, 2105 (2004).
45. J. Chakhalian *et al.*, *Nat. Phys.* **2**, 244 (2006).
46. J. Chakhalian *et al.*, *Science* **318**, 114 (2007).
47. Z. Sefrioui, *et al.*, *Appl. Phys. Lett.* **81**, 4568 (2002).
48. Z. Sefrioui *et al.*, *Phys. Rev. B* **67**, 214511 (2003).
49. V. Peña *et al.*, *Phys Rev. B* **69**, 224502 (2004).
50. A. I. Buzdin, *Rev. Mod. Phys.* **77**, 935 (2005).
51. F. S. Bergeret, A. F. Volkov and K. B. Efetov, *Rev. Mod. Phys.* **77**, 1321 (2005).
52. J. Y. Gu *et al.*, *Phys. Rev. Lett.* **89** , 267001 (2002).
53. A. Potenza and C. H. Marrows, *Phys. Rev. B* **71**, 180503(R) (2005).
54. R. Steiner and P. Ziemann, *Phys. Rev. B* **74**, 094504 (2006).
55. I. C. Moraru, W. P. Pratt Jr. and N. O. Birge, *Phys. Rev. Lett.* **96**, 037004 (2006).
56. A. Y. Rusanov *et al.*, *Phys. Rev. Lett.* **93**, 057002 (2004).
57. A. Singh, C. Sürgers and H. V. Löhneysen, *Phys. Rev. B* **B75**, 024513 (2007).
58. D. Stamopoulos, E. Manios and M. Pissas, *Supercond. Sci. Technol.* **20**, 1205 (2007).
59. G.-X. Miao, A. V. Ramos and J. S. Moodera, *Phys. Rev. Lett.* **101**, 137001 (2008).
60. J. Zhu *et al.*, *Phys. Rev. Lett.* **103**, 027004 (2009).
61. S. Soltan, J. Albrecht and H. U. Habermeier, *Phys. Rev. B* **70**, 144517 (2004).
62. T. Hu *et al.*, *Phys. Rev. B* **80**, R060506 (2009).
63. C. Visani *et al.*, *Nat. Phys.* **8**, 539 (2012).
64. M. Varela *et al.*, *Phys. Rev. Lett.* **83**, 3936 (1999).
65. M. Varela *et al.*, *Phys Rev. Lett.* **86**, 5156 (2001).
66. X. J. Chen *et al.*, *Phys. Rev. B* **72**, 104403 (2005).
67. Z. Sefrioui *et al.*, *Phys. Rev. B* **60**, 15423 (1999).
68. Z. Sefrioui *et al.*, *Europhys. Lett.* **48**, 679 (1999).
69. T. Endo *et al.*, *Phys. Rev. B* **54**, R3750 (1996).
70. V. Peña *et al.*, *Phys. Rev. Lett.* **97**, 177005 (2006)
71. M. Varela *et al.*, *Solid State Electron.* **47**, 2245 (2003).
72. A. Hoffmann *et al.*, *Phys. Rev. B* **72**, R140407 (2005).
73. J. W. Freeland *et al.*, *J. Phys. Cond. Mat.* **19**, 315210 (2007).
74. C. Visani *et al.*, *Phys. Rev. B* **81**, 094512 (2010).
75. R. Werner *et al.*, *Phys. Rev. B* **82**, 224509 (2010).
76. Z. L. Zhang *et al.*, *Appl. Phys. Lett.* **95**, 242505 (2009).
77. S. R. Giblin *et al.*, *Phys. Rev. Lett.* **109**, 137005 (2012).
78. J. Y. Gu *et al.*, *Phys. Rev. Lett.* **89**, 267001 (2002).
79. A. Potenza and C. H. Marrows, *Phys. Rev. B* **71** , 180503(R) (2005).
80. R. Steiner and P. Ziemann, *Phys. Rev. B* **74**, 094504 (2006).
81. I. C. Moraru, W. P. Pratt Jr. and N. O. Birge, *Phys. Rev. Lett.* **96**, 037004 (2006).
82. A. Yu. Rusanov, S. Habraken and J. Aarts, *Phys. Rev. B* **73**, 060505 (2006).
83. A. Singh, C. Sürgers and H. V. Löhneysen, *Phys. Rev. B* **75**, 024513 (2007).
84. G.-X. Miao, A. V. Ramos and J. S. Moodera, *Phys. Rev. Lett.* **101**, 137001 (2008).
85. V. Peña *et al.*, *Phys Rev. Lett.* **94**, 57002 (2005).
86. V. Peña *et al.*, *Phys Rev. B* **73**, 104513 (2006).
87. C. Visani *et al.*, *Phys. Rev. B* **75**, 54501 (2007).
88. N. M. Nemes *et al.*, *Phys. Rev. B* **78**, 094515 (2008).

89. N. M. Nemes *et al.*, *Phys. Rev. B* **81**, 024512 (2010).
90. C. Visani *et al.*, *Phys. Rev. B* **81**, 094512 (2010).
91. N. M. Nemes *et al.*, *Appl. Phys. Lett.* **97**, 032501 (2010).
92. J. Zhu *et al.*, *Phys. Rev. Lett.* **103**, 027004 (2009)
93. D. Stamopoulos, E. Manios and M. Pissas, *Phys. Rev. B* **75**, 014501 (2007).
94. K. Dybko *et al.*, *Euro Phys. Lett.* **85**, 57010 (2009).
95. W. Gillijns *et al.*, *Phys. Rev. Lett.* **95**, 227003 (2005).
96. L. Y. Zhu, T. Y. Chen and C. L. Chien, *Phys. Rev. Lett.* **101**, 017004 (2008).
97. Y. Liu *et al.*, *Phys. Rev. Lett.* **108**, 207205 (2012).
98. J. Salafranca and S. Okamoto, *Phys. Rev. Lett.* **105**, 256804 (2010).
99. S. Okamoto, *Phys. Rev. B* **82**, 024427 (2010).
100. C. Ulrich *et al.*, *Phys. Rev. Lett.* **103**, 107205 (2009).
101. B. Keimer *et al.*, *Phys. Rev. Lett.* **85**, 3946 (2000).
102. G. Khaliullin and S. Maekawa, *Phys. Rev. Lett.* **85**, 3950 (2000).
103. M. W. Haverkort *et al.*, *Phys. Rev. Lett.* **94**, 056401 (2005).
104. T. Mizokawa and A. Fujimori, *Phys. Rev. B* **54**, 5368 (1996).
105. J. Garcia-Barriocanal *et al.*, *Adv. Mat.* **22**, 627 (2010).
106. J. Garcia-Barriocanal *et al.*, *Nat. Commun.* **1**, 82 (2010) doi:10.1038/ncomms1080.
107. A. Tebano *et al.*, *Phys. Rev. Lett.* **100**, 137401 (2008).
108. F. Y. Bruno *et al.*, *Phys. Rev. Lett.* **106**, 147205 (2011).
109. J. H. Park *et al.*, *Nature* **392**, 794 (1998).
110. M. Bowen *et al.*, *Appl. Phys. Lett.* **82**, 233 (2003).
111. M. Izumi *et al.*, *Phys. Rev. B* **64**, 064429 (2001).
112. J. Z. Sun *et al.*, *Appl. Phys. Lett.* **73**, 1008 (1998).
113. C. T. Chen *et al.*, *Phys. Rev. Lett.* **75**, 152 (1995).
114. S. Valencia *et al.*, *Nat. Mater.* **10**, 753 (2011).
115. C.-G. Duan, S. S. Jaswal and E. Y. Tsymbal, *Phys. Rev. Lett.* **97**, 047201 (2006).
116. M. Fechner *et al.*, *Phys. Rev. B* **78** , 212406 (2008).
117. M. Fechner, S. Ostanin and I. Mertig, *Phys. Rev. B* **80**, 094405 (2009).
118. H. L. Meyerheim *et al.*, *Phys. Rev. Lett.* **106**, 087203 (2011).
119. P. Yu *et al.*, *Phys. Rev. Lett.* **105**, 027201 (2010).
120. M. Salluzzo *et al.*, *Phys. Rev. Lett.* **102**, 166804 (2009).
121. D. A. Dikin *et al.*, *Phys. Rev. Lett.* **107**, 056802 (2011).
122. A. X. Wang *et al.*, *Nature Commun.* **2**, 188 (2011).
123. L. Li *et al.*, *Nat. Phys.* **7**, 762 (2011).
124. J. A. Bert *et al.*, *Nat. Phys.* **7**, 767 (2011).
125. P. Moetakef *et al.*, *Phys. Rev. X* **2**, 21014 (2012).
126. M. R. Fitzsimmons *et al.*, *Phys. Rev. Lett.* **107**, 217201 (2011).
127. M. Gibert *et al.*, *Nat. Mater.* **11**, 195 (2012).
128. D. K. Satapathy *et al.*, *Phys. Rev. Lett.* **108**, 197201 (2012).
129. J. W. Seo *et al.*, *Phys. Rev. Lett.* **105**, 167206 (2010).
130. V. Garcia *et al.*, *Nature* **460**, 81 (2010).
131. A. Gruverman *et al.*, *Nano Lett.* **9**, 3539 (2009).
132. P. Maksymovych *et al.*, *Science* **324**, 1421 (2009).
133. V. Garcia *et al.*, *Science* **327**, 1106 (2010).
134. A. Chanthbouala *et al.*, *Nat. Nanotech.* **7**, 101 (2012).
135. Y. W. Yin *et al.*, *Nat. Mater.* **12**, 397 (2013)
136. Z. Sefrioui *et al.*, *Adv. Mat.* **22**, 5029 (2010).